Nuclear Physics B281 (1987) 365–380
North-Holland, Amsterdam

MEASUREMENT AND QCD ANALYSIS OF THE PHOTON STRUCTURE FUNCTION $F_2(x, Q^2)$

PLUTO Collaboration

Ch. BERGER, H. GENZEL, W. LACKAS, J. PIELORZ[1], F. RAUPACH and W. WAGNER[2]

I. Phys. Institut der RWTH Aachen[3], Fed. Rep. of Germany

A. KLOVNING and E. LILLESTÖL

University of Bergen[4], Norway

J. BÜRGER, L. CRIEGEE, A. DEUTER, F. FERRAROTTO[5], G. FRANKE, M. GASPERO, Ch. GERKE, G. KNIES, B. LEWENDEL, J. MEYER, U. MICHELSEN, K.H. PAPE, B. STELLA[5], U. TIMM. G.G. WINTER, M. ZACHARA[6] and W. ZIMMERMANN

Deutsches Elektronen-Synchrotron (DESY), Hamburg, Fed. Rep. of Germany

P.J. BUSSEY, S.L. CARTWRIGHT[7], J.B. DAINTON[8], D. HENDRY, B.T. KING[8], C. RAINE, J.M. SCARR, I.O. SKILLICORN, K.M. SMITH and J.C. THOMSON[9]

University of Glasgow[10], UK

O. ACHTERBERG, V. BLOBEL, D. BURKART, K. DIEHLMANN, M. FEINDT, H. KAPITZA[11], B. KOPPITZ, M. KRÜGER[12], M. POPPE, H. SPITZER and R. VAN STAA

II. Institut für Experimentalphysik der Universität Hamburg[3], Fed. Rep. of Germany

[1] Deceased.
[2] Now at University of California at Davis, Davis, Ca., USA.
[3] Supported by the BMFT, Fed. Rep. of Germany.
[4] Partially supported by The Norwegian Council for Science and the Humanities.
[5] Rome University, partially supported by INFN, Sezione di Roma, Italy.
[6] Institute of Nuclear Physics, Cracow, Poland.
[7] Now at Rutherford Appleton Laboratory, Chilton, UK.
[8] Now at University of Liverpool, Liverpool, UK.
[9] Now at Computing Laboratory, University of Strathclyde, Glasgow, UK.
[10] Supported by the UK Science and Engineering Research Council.
[11] Now at Carleton University, Ottawa, Ontario, Canada.
[12] Now at Universität Karlsruhe, Fed. Rep. of Germany.

0550-3213/87/$03.50

C.Y. CHANG, R.G. GLASSER, R.G. KELLOGG, S.J. MAXFIELD[13], R.O. POLVADO[14], B. SECHI-ZORN[1], J.A. SKARD, A. SKUJA, A.J. TYLKA, G.E. WELCH and G.T. ZORN

University of Maryland[15], USA

F. ALMEIDA[16], A. BÄCKER, F. BARREIRO[17], S. BRANDT, K. DERIKUM[18], C. GRUPEN, H.J. MEYER, H. MÜLLER, B. NEUMANN, M. ROST, K. STUPPERICH and G. ZECH

Universitäts-Gesamthochschule Siegen[3], Fed. Rep. of Germany

G. ALEXANDER, G. BELLA, Y. GNAT and J. GRUNHAUS

University of Tel-Aviv[19], Israel

H. JUNGE, K. KRASKI, C. MAXEINER, H. MAXEINER, H. MEYER and D. SCHMIDT

Universitäts-Gesamthochschule Wuppertal[3], Fed. Rep. of Germany

Received 8 July 1986

We present a measurement of the hadronic structure function $F_2^\gamma(x, Q^2)$ of the photon in the Q^2 range from 10 to 100 GeV^2. Data were taken with the PLUTO detector at the e^+e^- storage ring PETRA. This measurement and previous PLUTO measurements in the Q^2 range of 1.5 to 16 GeV^2 are compared with higher order QCD calculations. The structure function is consistent with the predicted $\log Q^2$ behaviour when charm contributions are subtracted. The x dependence can be well described for $0.1 < x < 0.9$ by the regularization scheme of Antoniadis and Grunberg. Within their scheme the data yield a value of $\Lambda_{\overline{\text{MS}}} = 183 + 65/-40(\text{stat.}) + 46/-36(\text{sys.})$ MeV for the QCD scale parameter.

1. Introduction

The reaction

$$ee \rightarrow ee + \text{hadrons} \tag{1}$$

proceeds mainly through the collision of two virtual photons. If one photon – the probe photon γ^* – is highly virtual ($Q^2 = -(\gamma^*)^2 \gg m_\rho^2$, with m_ρ = mass of the ρ meson), and the other photon – the target photon γ – is almost real ($P^2 = -(\gamma)^2 \ll m_\rho^2$), reaction (1) can be interpreted as deep inelastic electron scattering off predominantly transversely polarized photons [1]. In the present experiment, one

[13] Now at University of Massachusetts, Amherst, Mass., USA.
[14] Now at Northeastern University, Boston, Mass., USA.
[15] Partially supported by the Department of Energy, USA.
[16] On leave of absence from Inst. de Fisica, Universidad Federal do Rio de Janeiro, Brasil.
[17] On leave of absence from Universidad Autonoma de Madrid, Spain.
[18] Now at BESSY, Berlin, Fed. Rep. of Germany.
[19] Partially supported by the Israeli Academy of Sciences and Humanities–Basic Research Foundation.

electron (positron) is scattered and measured at large angles ($19° < \theta_T < 39°$); it is the source of the probe photon and will be called the tagging electron. As long as the scattering angle θ of the other electron which emitted the target photon γ is small ($\theta \leqslant \theta^{max} \ll 1$), and $W^2 = (\gamma^* + \gamma)^2 \gg P^2$, the cross section for reaction (1) factorizes [2,3] into an $e\gamma$ cross section and a target photon flux $N(z, \theta^{max})$ [1], which depends on the fractional energy $z = E_\gamma/E$ ($E = E_{beam}$) and the maximum electron angle. The deep inelastic $e\gamma$ cross section has contributions from the exchange of transverse and longitudinal virtual photons, and the cross section for reaction (1) can be written in terms of two structure functions, F_2 and F_L, and the flux of the (target) photon.

$$\frac{d\sigma}{dz\,dx\,dQ^2} = \frac{4\pi\alpha^2}{Q^4}\frac{1}{2x}\left\{\left(1+(1-y)^2\right)F_2(x,Q^2) - y^2F_L(x,Q^2)\right\}N_\gamma(z,\theta^{max}). \tag{2}$$

The scaling variables y and x are determined by the energy E_T, and the angle θ_T of the tagging electron and the mass W of the hadronic system:

$$y = 1 - (E_T/E)\cos^2\left(\tfrac{1}{2}\theta_T\right),$$

$$x = Q^2/(Q^2 + W^2).$$

The term y^2F_L in eq. (2) can be estimated to be small compared to the F_2 term. F_2 can therefore be determined directly from measurements.

If Q^2 is larger than a few GeV^2, hadron production in $\gamma^*\gamma$ interactions appears to proceed largely through the electromagnetic coupling of the probe photon to the charges of the virtual constituents (partons) of the target photon, in contrast to $Q^2 \lesssim 1$ GeV^2, where the interaction appears as the collision of two virtual vector mesons [4–6].

In the parton picture, the structure function $F_2(x)$ is proportional to the momentum and squared charge weighted parton distribution function in the target photon. QCD calculations for F_2 can be decomposed [5] into a perturbative term due to the $\gamma \to q\bar{q}$ splitting of the target photon (the point-like term) and a non-perturbative part. The latter is usually interpreted as the hadronic component of the photon and is estimated using VDM arguments [6,7]. The point-like part has been calculated in the quark-parton-model (QPM) [1] and in perturbative QCD, to leading order [8] and to higher order [9–13]. Two properties of the structure function have been predicted: its Q^2 evolution and – with some additional assumptions – also its magnitude within a limited x-range. Both the Q^2 evolution and the magnitude of $F_2(x, Q^2)$ depend on the QCD scale parameter Λ. However, to infer a reasonably precise value for Λ from the Q^2 evolution of F_2 alone, experiments with statistics much higher than presently available would be necessary.

In sects. 2 and 3 we present a measurement of the structure function $F_2(x)$ in the Q^2 range 18 to 100 GeV^2. In sect. 4 we use these and previously published results [14] at lower Q^2 values (1.5 to 16 GeV^2) to determine Λ using the QCD predictions [11] for the magnitude of $F_2(x, Q^2)$. The large Q^2 range of the combined measurements (1.5 to 100 GeV^2) allows the predicted Q^2 evolution to be checked.

2. Selection of high Q^2 tagged events

The data were obtained with the PLUTO detector [3,15] at the e^+e^- storage ring PETRA, running at beam energies of 17.3 GeV, during the period 1981 to 1982. The total evaluated luminosity was 40.1 pb^{-1}.

Deep inelastic eγ events were triggered inclusively by electrons scattered at angles θ from 19° to 39° into the end cap (EC) shower counter. Shower energies above 3 GeV were sufficient to trigger the detector.

To select the EC tagged multihadron events we adopt a procedure similar to that used in a previous analysis of events tagged by the large angle tagger ($5° < \theta < 15°$) at lower Q^2 [14]. Because the background contributions are larger at the EC tagging angles we have to impose slightly tighter cuts for event acceptance.

2.1. TAG DEFINITION AND CALIBRATION OF THE ENDCAP TAGGER (ECT)

The EC shower counter has a thickness of 10.3 radiation lengths over the polar angular region θ from 16° to 39°. In the azimuthal angle φ it is segmented into 30 equal sectors ($\Delta\varphi = 12°$). After 2.5 radiation lengths each sector is interleaved with one proportional chamber with a wire spacing of $\Delta\theta = 1°$.

Tracks are reconstructed using the interaction point, the EC proportional chamber and at least 2 central detector track chambers. This permits track recognition down to $\theta = 19°$. It was required that the lateral spread of the tagging shower was no broader than observed in Bhabha events (not more than 3 adjacent sectors), and that a track pointed towards the shower center within $\Delta\theta = 6°$. The direction (θ, φ) of the tagging electron was taken from the reconstructed track, and its energy from the shower counter. The shower energy resolution was $\Delta E/E = 6.8\%$ at beam energy, and the polar angle was resolved to $\pm 0.5°$. The Q^2 resolution, on average 9%, is mainly determined by the energy resolution.

The tagging efficiency for the ECT was determined from simulated eγ events. It was cross checked with data by selecting tags from real and simulated Bhabha events where cross sections are known. Both samples gave the same fraction of accepted tags within 1%. The ECT provides an entirely inclusive trigger for all eγ events with $E_T \geqslant 3$ GeV. After rejection of clean Bhabha events a total of 3354 events with $E_T > 8$ GeV was found.

2.2. BACKGROUND REJECTION

Most of the 3354 events accepted by inclusive EC tagging are still background from QED processes and from e^+e^- annihilation. The following cuts were applied to further reject background:

(i) A "clean tag" was required by allowing no further track near the tagging track, i.e. at $\theta < 45°$ on the same EC side and within an azimuthal angle relative to the shower center of $\Delta\varphi = 20°$. This cut removes 80% of the tags faked by annihilation events.

(ii) Events with a second tagging shower of $E > 4$ GeV, in the small (1.5°–4°) and large (5°–15°) angle taggers on the opposite θ-side were rejected. This cut removes degraded Bhabha and double tag events, and defines $\theta^{\max}$.

(iii) To reject QED events it was required that the final state had at least one non-showering track with a momentum of $\geqslant 1.0$ GeV/c, or at least 3 tracks which were not positively identified as electrons. Events with fewer than 2 measured tracks were rejected. Two-track events were kept only if they had no identified electron or muon, and if their neutral shower pattern required more than a single photon.

(iv) Events were rejected if the hadronic system had a mass of $W_{\text{vis}} > 12$ GeV.

(v) The missing momentum p^{miss} had to be compatible with an unobserved high momentum electron escaping through the beampipe: $p_\perp^{\text{miss}} < 3$ GeV, and $p_z^{\text{miss}} > 6$ GeV opposite to the z-direction of the tagging electron. Fig. 1 shows the distribution of p_z^{miss} after the $p_\perp^{\text{miss}}$ cut, for data, and for a MC simulation or annihilation and $e\gamma$ scattering according to the QPM. At $p_z^{\text{miss}} > 6$ GeV there is only a small contamination by annihilation events.

The effects of these cuts were checked by visually scanning samples of rejected events, both in data and in simulated samples. After the cuts, 114 events remained. The acceptance efficiency of the cuts for $e\gamma$ events was determined to be 55% from simulated $e\gamma$ events as described below.

The contamination of the sample of 114 events was estimated using Monte Carlo simulations of the following reactions:

$e^+e^- \to$ hadrons	8.0 events,
$e^+e^- \to e^+e^-\tau\tau$	11.1 events,
$e^+e^- \to e^+e^-$ + hadrons via the Compton diagrams from virtual bremsstrahlung	4.8 events.

Other background sources, like $e^+e^- \to \tau\tau$ or beam gas events were found to be negligible.

The Monte Carlo simulation predicts that only 0.05% of annihilition events, equivalent to 8 events, will pass the $e\gamma$ cuts. This prediction can be checked with the data at $p_z^{\text{miss}} < 2.0$ GeV/c. Fig. 1 shows that almost no $e\gamma$ events are expected for $p_z^{\text{miss}} < 2.0$ GeV/c, while annihilation events giving false tags peak near $p_z^{\text{miss}} = 0$.

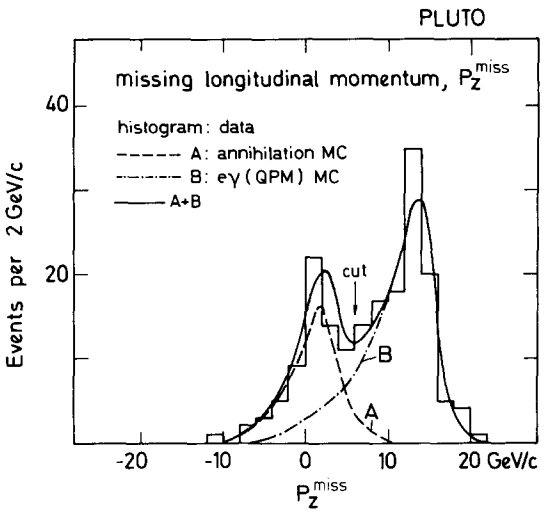

Fig. 1. Missing p_z distribution from data, and Monte Carlo (MC) simulations for $e\gamma \to e + \text{hadrons}$ (QPM) and $e^+e^- \to \text{hadrons}$. P_Z^{miss} is the momentum missing along beam direction opposite to the observed tag.

Hence the data at $p_z^{miss} < 2.0$ GeV can be used to (re-)calibrate the predicted rejection efficiency for annihilation events by the eγ event selection cuts. This method gives a background of 6.2 events. A visual inspection of the 114 accepted events yielded 9 events which were clearly identified as e^+e^- annihilation events on the basis of obvious back-to-back 2-jet topology with one jet simulating a tag. The 9 events were removed from the data sample instead of performing a statistical subtraction.

The τ pair and the Compton backgrounds are events with a real tagging electron. They cannot be further distinguished from the other eγ events and were subtracted statistically.

3. Determination of the photon structure function

To evaluate $F_2(x, Q^2)$ from the accepted events after background subtraction we have to

(1) correct for losses of eγ events due to the background rejection cuts,

(2) invert the detector dependent "smearing" $x \to x_{vis}$ introduced by particle losses and resolution,

(3) correct for effects of radiative and other higher order processes.

To exclude badly reconstructed events from the $x_{vis} \to x$ unfolding, only those 89 events with charge balance better than ± 3 and the observed hadronic mass $W_{vis} > 1.5$ GeV were used. Furthermore, we neglected the term with F_L in eq. (2).

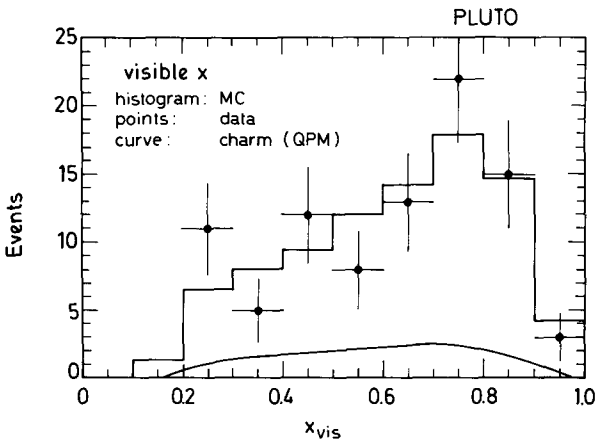

Fig. 2. x_{vis} distribution. The MC uses the unfolded structure function $F_2(x)$.

Its contribution depends on the unknown ratio F_L/F_2, and a model is required. At the average Q^2 of the data, $\langle Q^2 \rangle = 45$ GeV^2, we find $F_L/F_2 = 0.16$ from the QPM. The F_L term contributes less than 2% to the cross section in the accepted kinematic region. No correction is applied to F_2 for neglecting the F_L term. Corrections (1), (2) and (3) are incorporated in an unfolding procedure.

In this procedure Monte Carlo events were generated according to eq. (2) with an appropriate hadronization model. $F_2(x, Q^2)$ is factorized into a Q^2 interpolating function and $F_2(x, Q^2 = \langle Q^2 \rangle)$ [14]. $F_2(x, \langle Q^2 \rangle)$ was set to unity at the event generation step. The simulated events were then weighted with a smooth weight function $w(x)$ such that the observed x_{vis} distribution (fig. 2) was best reproduced. The quantity $w(x)$ is then the unfolded structure function $F_2(x, \langle Q^2 \rangle)$. Further details are given in refs. [14, 16].

Since QCD calculations are performed for massless quarks, i.e. without threshold effects, we present also a "charm-subtracted" structure function for QED comparisons. Here the contribution from heavy charm quark production to the F_2 structure function is estimated using the QPM, and subtracted from the measured structure function.

3.1. MODELLING THE HADRONIC FINAL STATE

For hadronization of the $\gamma^*\gamma$ system we have used a Lorentz invariant all-pion phase space model (IP), and a special quark model (QM). The latter differed from the standard QPM in so far as only the angular distribution of the process $\gamma^*\gamma \to q\bar{q}$ was taken from QED while the total cross section was adjusted to give $F_2(x) = 1$ for all x. The quarks were then fragmented according to the Feynman-Field scheme [17]. The fragmentation parameters for the phase space model were the same as in

[14]. Below $W = 3.5$ GeV the IP model was used and above $W = 7$ GeV the QM. In the intermediate W-region we used a linear transition from 100% IP to 100% QM. We have checked that the average $x - x_{vis}$ shifts from both models are compatible.

In the Q^2 region of 18 to 100 GeV^2 charm quark production contributes to x-values up to 0.8. For these events we expect a fragmentation different from that for u- (and d-) quark events, with a larger $x - x_{vis}$ shift. MC studies yielded $\langle x - x_{vis} \rangle = 0.08$ for u-quark events, and $\langle x - x_{vis} \rangle = 0.13$ for events with charm quark decays, after their reconstruction in the PLUTO detector. To avoid an inappropriate unfolding of the expected charm contribution contained in the data we used the QPM to estimate the charm x_{vis} distribution (16% of the observed events) – shown as the curve in fig. 2 – and subtracted it from the observed x_{vis} distribution before the unfolding step. The resulting unfolded $F_2(x)$ will be called "charm subtracted". The complete $F_2(x)$ structure function was obtained by adding $F_2^{charm}(x)$ as given by the QPM.

The hadronic final state model satisfactorily reproduces the kinematic properties of the data that are important for the corrections (1) and (2) discussed above. This is illustrated in the distributions shown in fig. 3a–c:

(3a) the single charged particle transverse momentum p_T, with respect to the e^+e^- beam direction,

(3b) the charged particle multiplicity n_{ch}, and

(3c) the neutral energy E_n.

The normalization of the MC distribution is produced by the unfolded $F_2(x)$ structure function, and in fig. 3a additionally by the charged track multiplicity spectrum of the MC events.

In fig. 4 we show the measured distributions of (a) E_T, (b) Q^2 and (c) W_{vis}, together with the result of unfolding. Even though the distributions were not used to determine the unfolded structure function, they are well described by the hadronization model together with the unfolded $F_2(x, Q^2)$ solution.

3.2. RADIATIVE CORRECTIONS

Formula (2) for reaction (1) is derived in lowest order QED (LOQ). Radiation by the initial and final state electrons modifies the relation between $F_2(x, Q^2)$ and the measured cross section. We have investigated the size of radiative effects using a computer program by Berends et al. [18] and employing the QPM for the $\gamma^*\gamma \to$ hadrons transition. The effect is an increased cross section σ_{rad} as compared to σ_{LOQ}, at small tagging energies, which in turn leads to an increased cross section at small x, mainly at $x_{vis} \lesssim 0.4$. In total the rate of accepted events N_{rad} is larger than the lowest order rate, N_{LOQ}, by 6.9%. An exact procedure for the radiative correction of $F_2(x)$ is complicated. Since these effects are small, we have performed an approximate correction by weighting the measured x_{vis} distribution (fig. 2) with the event ratio $N_{LOQ}(x_{vis})/N_{rad}(x_{vis})$ in the unfolding step.

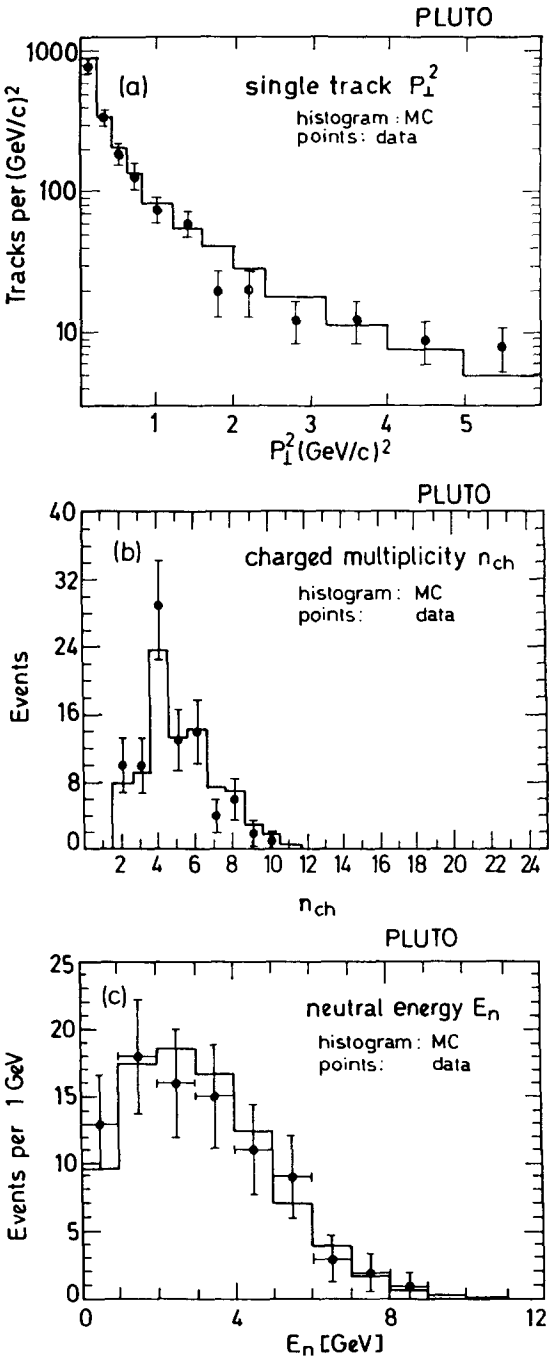

Fig. 3. Distributions relevant for acceptance corrections: (a) charged particle p_T^2, (b) charged particle multiplicity of events, n_{CH} (c) neutral energy of events, E_n. The MC uses the unfolded structure function $F_2(x)$.

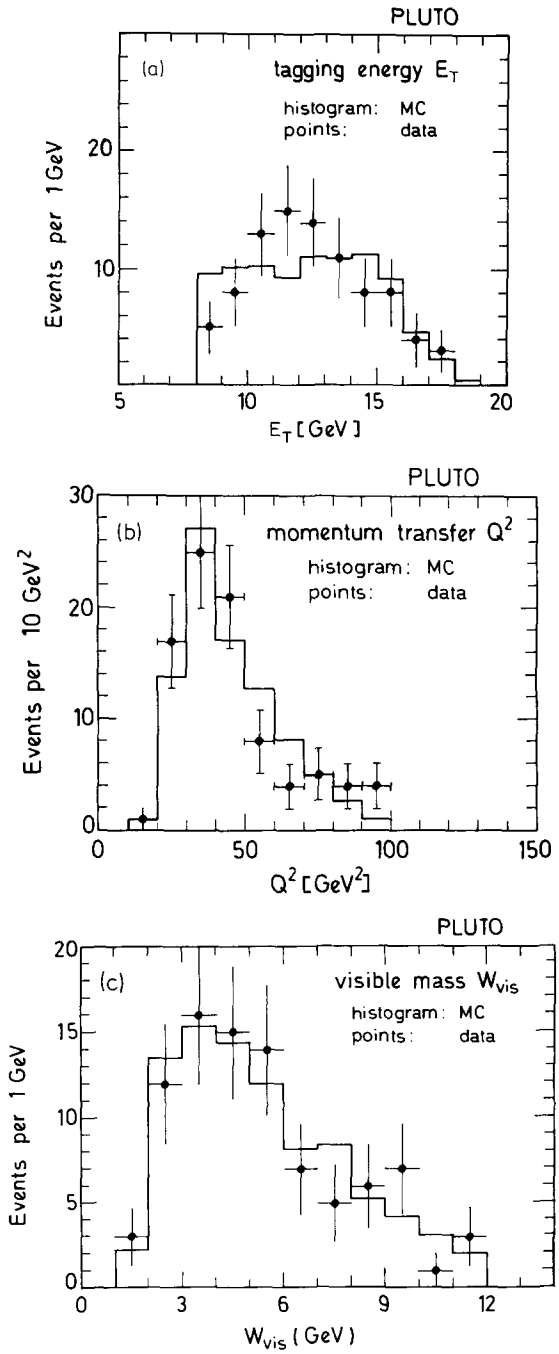

Fig. 4. Comparison of observed distributions with the result of unfolding (a) E_{tag}, (b) Q^2, (c) W_{vis}. The MC histograms are calculated with the unfolded structure function $F_2(x)$.

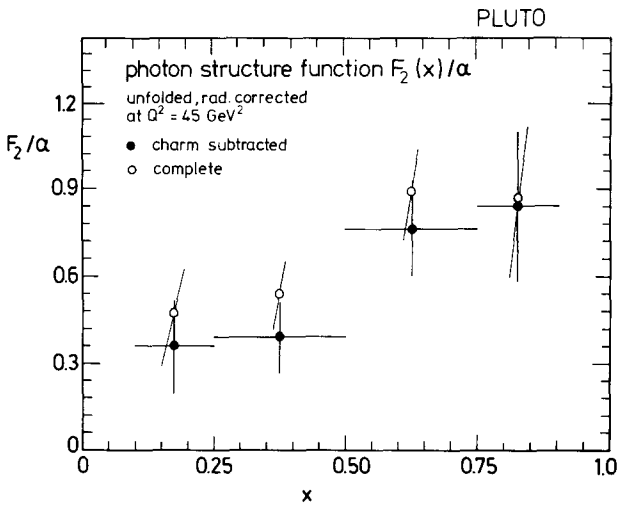

Fig. 5. The complete and the charm-substructured structure functions $F_2(x)$ at $Q^2 = 45$ GeV^2, unfolded and radiatively corrected.

3.3. RESULTS

The unfolded structure function with radiative corrections is shown in fig. 5, interpolated to the average Q^2 value of the data sample of $\langle Q^2 \rangle = 45$ GeV^2. The results for the complete and for the charm subtracted structure function are shown separately. Both rise with x.

All data points have an additional systematic error of 10% mainly due to uncertainties in the hadronization model employed in calculating acceptance corrections.

4. Comparison with QCD calculations

We use the results presented above and our previous F_2 measurements at lower Q^2 [14] for a comparison with QCD calculations and a determination of Λ. The basic properties predicted for the charm-subtracted photon structure function $F_2(x, Q^2)$ in leading [8] and higher [9–13] order QCD calculations, namely a rise with x and with Q^2 (approximately as $\ln(Q^2/\Lambda^2)$) are qualitatively observed in the data shown in figs. 5 and 6, respectively. In fig. 6, $\langle F_2(Q^2) \rangle$ is the charm-subtracted structure function, averaged over the x-interval 0.3–0.8.

For a quantitative test of QCD and for a determination of the QCD scale parameter Λ, a higher order calculation has to be used. The full solution of the higher order evolution equations for $F_2(x, Q^2)$, however, contains non-perturbative terms associated with the quark-antiquark wave function of the photon. This hadronic component cannot be calculated at present, but can be furnished as

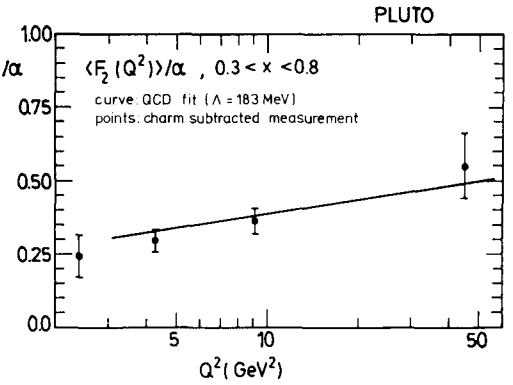

Fig. 6. $\langle F_2 \rangle$ at $Q^2 = 2.4$, 4.3, 9.2, 45 GeV^2, averaged for $0.3 < x < 0.8$. The points at $Q^2 = 2.4$, 4.3 and 9.2 GeV^2 are from [14]. The curve is from the QCD fit described in the text.

boundary conditions in terms of a known (measured or estimated) photon structure function at a specific value of Q^2 [12]. The full solution is then obtained by an evolution in Q^2 which depends on Λ. For a determination of Λ from the Q^2 evolution high accuracy data on F_2 are required over a large range of $\ln(Q^2)$. We have insufficient statistical accuracy to determine Λ using this procedure.

Another approach is to separate the full higher order solution for F_2 into a calculable perturbative term and a term which contains the incalculable hadronic pieces [5, 6, 8–11].

$$F_2(x, Q^2) = F_2^{\text{point}}(x, Q^2, \Lambda) + F_2^{\text{had}}(x, Q^2). \tag{3}$$

The calculable term, F_2^{point} is due to the point-like part of the photon. It grows with Q^2, dominates at asymptotic Q^2 values, and is referred to as the asymptotic solution. The asymptotic solution of the higher order evolution equation, however, is singular at $x = 0$ and negative for $x < 0.2$ [9, 10]. Since F_2 has to be positive and finite, F_2^{had} has also to contain a singularity to make the sum $F_2^{\text{point}} + F_2^{\text{had}}$ positive and finite. If one approximates the incalculable F_2^{had} by the usual estimate based on SU(3) and VDM [6, 7]:

$$F_2^{\text{VDM}}(x, Q^2) = 0.2\alpha(1 - x), \tag{4}$$

the singularity in F_2^{point} is obviously not cancelled.

Antoniadis and Grunberg [11] have proposed a regularization scheme for F_2^{point} to remove the divergence, which occurs in the second moment of F_2^{point}. They

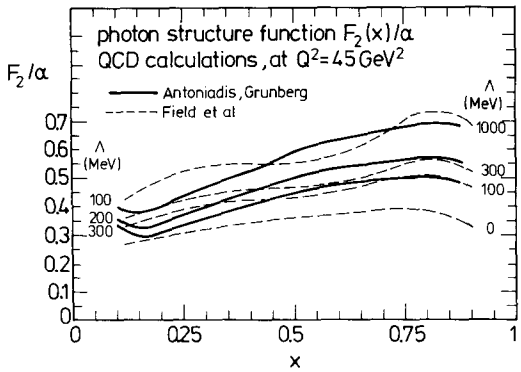

Fig. 7. Sensitivity of the photon structure functions F_2 to Λ. Solid lines show the Antoniadis-Grunberg approach [11] for $\Lambda_{\overline{\mathrm{MS}}} = 100$, 200 and 300 MeV and with $H = 0.018$ in eq. (6). Dashed lines are predictions from a Q^2 evolution calculation [13] for $\Lambda = 0$, 100, 300 and 1000 MeV.

modify this moment by adding an extra term which explicitly cancels the pole for $x \to 0$. The structure function then reads:

$$F_2(x, Q^2) = F_2^{\text{point,reg}}(x, Q^2, \Lambda, t) + F_2^{\text{had,reg}}(x, Q^2). \tag{5}$$

This decomposition differs from eq. (3) in so far as both terms are now finite and positive. $F_2^{\text{point,reg}}$, however, depends on a parameter t which is not determined perturbatively. For $t = 0$ eq. (3) is restored, and for $t > 0$ the shape of $F_2^{\text{point,reg}}(x)$ depends on $\ln(t)$, mainly at small x. At $x > 0.3$, $F_2^{\text{point,reg}}$ differs little from the original F_2^{point}. The sensitivity of $F_2^{\text{point,reg}}$ resulting from [11] to Λ is displayed in fig. 7. Here we show $F_2^{\text{point,reg}}$ for $\Lambda = 100$, 200 and 300 MeV, as solid lines. The dashed curves show predictions from a QCD-improved QPM to first order in α_s [13]. The two types of F_2 calculation are controversial, and the evolution approach [13] is too insensitive to Λ to allow a significant determination from our data. Therefore we evaluate Λ only in the Antoniadis-Grunberg scheme.

The incalculable $F_2^{\text{had,reg}}(x, Q^2)$ we assume to be proportional to the VDM estimate:

$$F_2^{\text{had,reg}}(x, Q^2) = H\alpha(1 - x). \tag{6}$$

The parameters Λ, $\ln(t)$ and h have been determined in a common fit to the data at $Q^2 = 4.3$, 9.2 and 45 GeV^2 as shown in fig. 8. For the QCD scale parameter within approach [11] we find

$$\Lambda_{\overline{\mathrm{MS}}} = 183 + 65/-40(\text{stat}) + 46/-36(\text{syst})\ \text{MeV}. \tag{7}$$

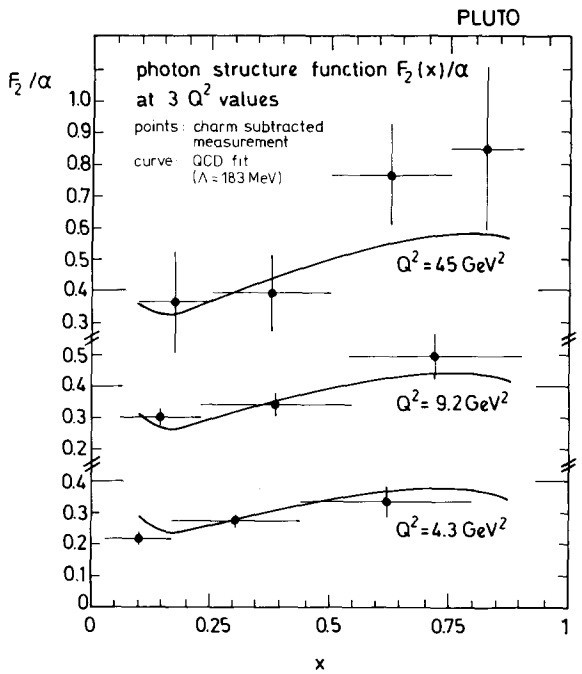

Fig. 8. Comparison of the QCD fit described in the text with the measured $F_2(x, Q^2)$. The data at $Q^2 = 4.3$ GeV^2 and 9.2 GeV^2 are from [14].

The value for Λ is only moderately correlated with the two non-perturbative parameters $\ln(t)$ and H (correlation coefficients $c(\Lambda, \ln(t)) = 0.36$, $c(\Lambda, H) = 0.18$). It turns out that these parameters are not well determined since they are strongly correlated ($\ln(t) = 0.8 \pm 0.16$, $H = 0.018 \pm 0.012$, correlation coefficient $c(\ln(t), H) = 0.87$). If the charm subtraction is altered by $\pm 20\%$, Λ is changed by only ± 1 MeV. If the VDM term (6) is parametrized as $Hx^{0.4}(1-x)^{1.1}$ [19] the fitted Λ differs from (7) by much less than the statistical error. The systematic error quoted above is dominated by uncertainties in the event acceptance calculations, and includes uncertainties from luminosity, radiative corrections and target mass effects.

Fig. 8 shows that the fitted $F_2(x)$ (solid curves) describes the data well at all three values of Q^2. The Q^2 dependence of the measured F_2, averaged over the interval $0.3 < x < 0.8$, is displayed in fig. 6. The QCD curve with $\Lambda_{\overline{\text{MS}}} = 183$ MeV adjusted to fit the absolute value of F_2 on average, also agrees well with the Q^2 dependence of F_2 from 4.3 to 45 GeV^2, and even with the data point at $Q^2 = 2.4$ GeV^2 which was considered to be too low in Q^2 to be included in the QCD fit.

The value of Λ found in this analysis of the reaction $e\gamma \to e + \text{hadrons}$ is consistent with that found in similar experiments [20], and in many other processes [21, 22].

5. Conclusions

We have presented new data for the photon structure function $F_2(x)$ at $Q^2 = 45\ \mathrm{GeV}^2$. The charm subtracted structure function at $Q^2 = 45\ \mathrm{GeV}^2$ together with previous measurements at $Q^2 = 9.2$ and $4.3\ \mathrm{GeV}^2$ have been analysed in terms of a divergence free higher order QCD prediction. The QCD scale parameter Λ in the point-like part and parametrizations for the unknown non-perturbative contributions have been fitted to the data. The x and Q^2 dependence of the data is well reproduced. Within the Antoniadis-Grunberg approach we find a value of

$$\Lambda_{\overline{\mathrm{MS}}} = 183^{+65+46}_{-40-36}\ \mathrm{MeV},$$

which is in good agreement with the results from other processes.

We wish to thank the members of the DESY directorate for the hospitality extended to the university groups. We are indebted to the PETRA machine group for having provided us with excellent beam conditions in 1981/82 and the DESY computer center for their efficient performance. We gratefully acknowledge the efforts of all the engineers and technicians who have contributed to the construction and maintenance of the apparatus.

References

[1] V.M. Budnev et al., Phys. Reports 15C (1975) 181; Yad. Phys. 13 (1971) 353
[2] Ch. Berger and J.H. Field, Nucl. Phys. B187 (1981) 585
[3] L. Criegee and G. Knies, Phys. Reports 83 (1982) 151
[4] PLUTO Collaboration, Ch. Berger et al., Z. Phys. C26 (1984) 191, 353;
G. Knies, The total cross section in $\gamma\gamma \to$ hadrons, Proc. 6th International Workshop on Photon-photon collisions, Granlibakken, Cal., USA (1984) p. 278; DESY report 84-122 (1985)
[5] C. Peterson, T.F. Walsh and P.M. Zerwas, Nucl. Phys. B174 (1980) 424
[6] C. Peterson, T.F. Walsh and P.M. Zerwas, Nucl. Phys. B229 (1983) 301
[7] W. Wagner, RWTH Aachen preprint PITHA 83/03 (1983)
[8] E. Witten, Nucl. Phys. B120 (1977) 189
[9] W.A. Bardeen and A.J. Buras, Phys. Rev. D20 (1979) 166
[10] D.W. Duke and J.F. Owens, Phys. Rev. D22 (1980) 2280
[11] I. Antoniadis and G. Grunberg, Nucl. Phys. B213 (1983) 445;
I. Antoniadis, private communication
[12] M. Glück and E. Reya, Phys. Rev. D28 (1983) 2749;
M. Glück, K. Grassi and E. Reya, Phys. Rev. D30 (1984) 1447
[13] J.H. Field et al., DESY report 86-046 (1986), submitted to Phys. Lett.; private communication
[14] PLUTO Collaboration, Ch. Berger et al., Phys. Lett. 142B (1984) 111
[15] L. Criegee and G. Knies, ref. [3];
PLUTO Collaboration, DESY internal report PLUTO 79-01 (PRC 79-06) (1979);
R.G. Kellogg et al., DESY internal report PLUTO 84-04 (1984);
S.L. Cartwright, thesis, DESY internal report PLUTO 84-01 (1984)

[16] V. Blobel, Unfolding methods in high energy physics experiments, 1984 CERN School of Computing, Aignablava (Spain);
A. Bäcker, Unfolding techniques, Proc. 6th International Workshop on photon-photon collisions, Granlibakken, Cal., USA, (1984) p. 205; DESY Report 84-118
[17] R.P. Feynman and R.D. Field, Nucl. Phys. B136 (1978) 1
[18] F. Berends, P.H. Daverfeldt and R. Kleiss, Instituut Lorentz, Leiden preprint (1984)
[19] NA3 Collaboration, J. Badier et al., Z. Phys. C18 (1983) 218
[20] JADE Collaboration, W. Bartel et al., Z. Phys. C24 (1984) 231;
TASSO Collaboration, M. Althoff et al., submitted to Z. Phys. C; DESY preprint 86-026 (1986)
[21] G.P. Lepage, Proc. 1983 Int. Symp. on Lepton and photon interactions at high energies. Cornell, Ithaca, USA (1983) p. 565
[22] R.-Y. Zhu; Caltech preprint, CALT-68-1306 (1985)